AVE Trends in Intelligent Applied Sciences

Hybrid Power Management Strategy Using SFO-Based Improved Sand Cat Swarm Optimization for Effective Fuel Economy in HEV Application

B. Gunapriya[1,*], N. Samanvitha[2], S. Venkatasubramanian[3], M. Arunadevi Thirumalraj[4], Bhopendra Singh[5]

[1]Department of Electrical and Electronics Engineering, New Horizon College of Engineering, Bengaluru, Karnataka, India.
[2]Department of Electrical and Electronics Engineering, Nitte Meenakshi Institute of Technology (NMIT), Bengaluru, Karnataka, India.
[3]Department of Computer Science and Business Systems, Saranathan College of Engineering, Tiruchirappalli, Tamil Nadu, India.
[4]Department of Computer Science and Engineering, Karunya Institute of Technology and Science, Coimbatore, Tamil Nadu, India.
[4]Department of Computer Science and Business Management, Saranathan College of Engineering, Tiruchirappalli, Tamil Nadu, India.
[5]Department of Engineering, Amity University Dubai, Dubai, United Arab Emirates.
gunapriyab@newhorizonindia.edu[1], samanvitha.n@nmit.ac.in[2], veeyes@saranathan.ac.in[3], aruna.devi96@gmail.com[4]
bhopendrasingh@yahoo.com[5]

*Corresponding author

Abstract: As the use of renewable energy increases, the electrical energy storage system must overcome several challenges. As battery technology improves, the range of electric cars (EVs) increases, driving rising demand for these vehicles. An efficient electrical energy storage expedient is required to address the issue of low-range EVs. Conventional electric cars rely on a single power source, which is inadequate for meeting the EV's varying energy needs. To accommodate the high energy density of EV loads, a novel storage medium is required. Fuel efficiency in a HEV is directly related to the PMS employed. In this research, the researchers propose a hybrid power management strategy that combines an SFC with the equivalent consumption minimisation approach (ECMS), with the SFC's hyperparameters tuned using Improved Sand Cat Swarm Optimisation (ISCSO). AI has been a game-changer in coordinating the needs of sources. The supply is a green technology that combines a PEMFC with batteries and ultracapacitors for additional energy storage. The model is developed using MATLAB/Simulink. The simulation-projection scheme meets the power demand of a typical cycle, while other PMS have been evaluated based on hydrogen consumption, overall efficiency, base, and DC bus stability.

Keywords: Power Management Strategy (PMS); Sugeno Fuzzy Controller (SFC); Electrical Energy Storage System; Artificial Intelligence (AI); MATLAB/Simulink; State Machine Control; Proton Exchange Membrane Fuel Cell (PEMFC).

Cite as: B. Gunapriya, N. Samanvitha, S. Venkatasubramanian, M. A. Thirumalraj, and B. Singh, "Hybrid Power Management Strategy Using SFO-Based Improved Sand Cat Swarm Optimization for Effective Fuel Economy in HEV Application," *AVE Trends in Intelligent Applied Sciences*, vol. 1, no. 2, pp. 76–95, 2025.

Journal Homepage: https://www.avepubs.com/user/journals/details/ATIAS

Received on: 17/06/2024, **Revised on:** 28/07/2024, **Accepted on:** 18/10/2024, **Published on:** 09/06/2025

DOI: https://doi.org/10.64091/ATIAS.2025.000178

1. Introduction

Due to environmental concerns and increasing petrol prices, EVs are gaining popularity. Electric vehicles (EVs) offer better fuel efficiency and meet current global emission standards than gasoline-powered internal combustion engine (ICE) cars. There are conventional electric vehicles on the market. EVs must meet considerable power requirements, such as rapid acceleration and deceleration. The battery's performance suffers because of the large transient charging current it must absorb during the period, which is equivalent to pulse load variations. In certain cases, an ultracapacitor is employed in addition to the battery to counteract this drain [1]. The impact of the battery's presentation on sudden draining can be reduced by using a variety of ultracapacitor connection topologies. Since the device is an ultracapacitor, it can manage an immediate impulse EV load, reducing the strain on the battery while increasing the high-rate current requirement. It is possible to fulfil peak power demand. When they are used together [2], [3]. To ensure the load's needs are met during the drive's sudden acceleration and deceleration/regenerative periods, ultracapacitors can provide and even absorb enormous power. An appropriate interface between the battery and the ultracapacitor is necessary due to fundamental differences between the two sources (e.g., voltage levels or charging/discharging). Battery-ultracapacitor combinations can boost EV performance in terms of power and energy density, as well as lifecycle, compared to either battery or ultracapacitor alone.

Battery life may be extended and energy consumption reduced, thanks to the enhanced Hybrid Energy Storage System (HESS) across various devices [4]. Our active HESS maximises the utilisation of ultracapacitors and batteries, enabling us to meet the fluctuating power demands of EVs [5]. An active HESS configuration maximises the Energy stored in ultracapacitors, leading to better fuel efficiency and increased energy security through the use of multiple sources. In Figure 1, researchers see the fundamental components of an EV drivetrain. The battery is the source that ensures the vehicle can travel the required distance. Since the curb weight of an EV is directly related to the tractive effort, reducing it is crucial [6]. Since they are smaller, lighter, require less upkeep, and have a longer lifespan than lead-acid and nickel-metal hydride batteries, lithium-ion (particularly lithium iron phosphate, or LFP) batteries are the current standard. Its energy density is between 90 and 120 Wh/kg. The LFP battery has a lifespan of 1000-2000 cycles. UC has an exact power of up to 10,000 W/kg, an exact energy of around 5 Wh/kg, and a far longer lifespan of almost a million cycles [7]. When discharging or charging, the multi-input bidirectional converter determines how much power comes from the battery and how much comes from the UC. For forward power flow, it operates in boost mode; for reverse power flow, it operates in buck mode.

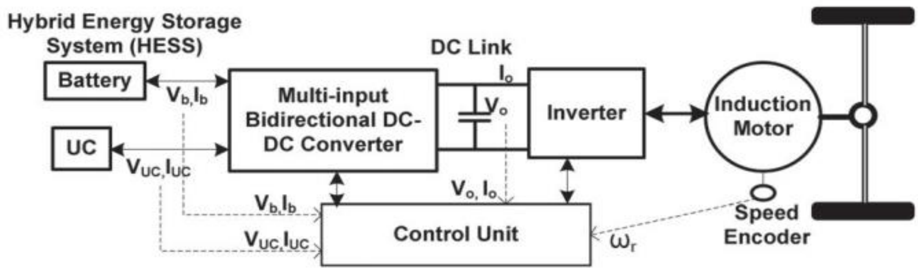

Figure 1: Block diagram of a typical EV powertrain

The ultracapacitor and battery in a hybrid source don't have identical charging, discharging, voltage, and other fundamental characteristics; hence, an appropriate interface is required. For a more efficient and effective distribution of the system across energy storage devices, a strategy (also known as HESS) is necessary [8]. This is because a bidirectional DC-DC converter can satisfy the criteria for high utilisation efficiencies. State of charge and power output from the source are the only two states in which active power management operates. Therefore, including an ultracapacitor in the system adds a new control variable that has a degree of freedom. This additional state makes it harder to develop and optimise active power management [9]; [10]. By combining the compensations of batteries and ultracapacitors, researchers may minimise costs by safeguarding batteries and optimising the size of both energy storage devices [11]. Fuzzy-logic control, rule-based, model-predictive, and filtration-based HESS management methods, among others, have been presented over time [12]; [13]. A rule-based HESS approach may be used to concurrently regulate the size limitations and power management of an EV's individual system, which incorporates diverse components [14].

Despite the following compensations, these units increase load on the power grid, and the charging or discharging of several electric vehicles can aggravate power demand during peak hours [15]. Because of this, a system to coordinate charging and discharging for a home's electric vehicle (EV) fleet and ESU is essential. The proposed HESS system is put through its paces by simulating a miniature EV load profile utilising this industry-standard actual drive and the EV dynamic model. The generated load profile is then applied to the system, and the MATLAB/Simulink simulation results are analysed. In this investigation, several rule-based active HESS schemes were employed to lessen the impact of a single power source’s limitation (low energy density).

2. Relate the Whole Thing

For EMS testing and the assessment of fuel ingesting, pollutant releases (CO and THC), Estrada et al. [16] provide an approach for constructing hybrid models. In this setting, the strong influence of transients makes it challenging to measure pollutant emissions with static models, such as the popular map-based technique. The main influence of this article is the use of Convolutional Neural Networks (CNN) to accurately characterise pollutant emissions, both in the short term and over time. All examples of traditional ICE input parameters. The suggested CNNs are minimised for simplicity and computational speed. Experimental data from chassis dyno testing of a regular turbocharged gasoline-powered car is used to inform the development of these vehicles. Real- of the entire HEV vehicle is made possible by combining the pollutant emission models of the remaining powertrain. In this paper, researchers present the Double Deep-Q learning method for the EMS and compare it with the Dynamic solution. A co-simulation framework using MATLAB-Simulink and AMESIM is used to develop the described technique. The resultant model is 8- to 10-times quicker than real-time in a typical desktop computer. This allows for the creation of models that can be used in the loop scenarios. The total cumulative error for pollutants, including CO and HC emissions, is less than 8.5 percent, while the total error for anticipated CO2 is below 2.5 percent. To help establish the system effect of the doubts, Alsharif et al. [17] suggest the use of the Stochastic Method (SMCM). By studying the influence of an unknown number of EVs on household power in Libya, and scaling the organisation's shape algorithm, this research aims to acquire a cost-effective system. The electric power system is modelled using Strategy (RB-EMS), while the optimal sum of sources is determined.

The expected impact was determined following a sensitivity analysis. Results from the size, control, and sensitivity analyses are the primary focus of this discussion. Zhang et al. [18] propose an ACC-EMS method grounded in hierarchical reinforcement learning but employing non-hierarchical execution. Low-level policy learns to achieve the required objectives by adjusting the variable quantity implemented by the host vehicle. In contrast, the high-level policy learns to generate trajectories in terms of headway. The proposed ACC-EMS approach uses I-880 GPS data to learn from a car-following situation. Extensive simulations showed that our proposed method significantly outperformed the offline global optimum in terms of training speed and stability, while having a smaller impact on energy consumption and requiring fewer computer resources. To achieve optimal energy bases in the two modes, as established by Huang et al. [19], this study presents a dual deep algorithmic framework, the first of its kind. A prior-action guidance strategy is also described to help networks better approximate the action-value function during training. Data from training shows that reusing the same action guiding mechanism improves learning in two ways: exploration. The authentication results show that the proposed approach significantly reduces fuel cell lifetime loss, bringing the average fluctuation in fuel cell output below 100 W. Research into the new framework, patterns, and energy management strategy is encouraged. Liu et al. [20] propose an imitation reinforcement learning technique with optimal guidance for energy-control vehicles to accelerate the solution process and concurrently achieve desired control performance. First, an offline global optimisation method is used to determine power-allocation trajectories that account for a range of driving scenarios. To generate high-efficiency solutions, reinforcement learning is combined with optimal trajectories during training, and constraints on battery depletion relative to driving distance are added to create a constrained state space.

Computer simulation results show that the projected approach is superior to other methods for reducing energy consumption in HEVs across an extensive range of driving conditions, and it can also serve as a useful solution roadmap for similar problems in constrained and optimum mechanical and electrical systems. Sun et al. [21] proposed an EMS that combines deep learning with high-quality model predictive control to more effectively regulate energy consumption. First, an energy flow test was used to validate a mechanical, electrical, thermal, and hydraulic (METH) model of the PHEV. Second, researchers constructed and compared six prediction models using a wide range of methods. Under the Worldwide Light-duty, the impacts of three EMSs and LSTM-IMPC were evaluated. These findings reveal that the LSTM-IMPC-based EMS saves gasoline by 3.81%, 5.61%, and 18.71% compared to the CD-CS-based EMS across these three cycles, respectively, demonstrating the significant advantage of the proposed EMS. The LSTM-IMPC-based EMS yields fuel savings rates that are extremely close to those of the DP-based ideal during cycles. Abd-Elhaleem et al. [22] present an improved power management method for PHEVs. This approach consists of a smart controller for the near term and a power management strategy for the far future. For sustained efficiency, a chaotic enhanced generalised particle swarm optimisation (CIGPSO) technique is used to optimise the torques of electric motors and diesel generators. In hybrid mode, where power is split between an electric motor and an internal combustion engine, the CIGPSO uses a five-mode rule-based control scheme to determine optimal torques for the motor and engine while minimising total computational cost.

This cost function minimises gasoline use while simultaneously minimising battery current draw and accounting for battery ageing. As the battery is charged and drained along the route, the CIGPSO may also record the battery's SoC curve. The fuzzy (IT2TSK) algorithm, which relies on human professionals, is used to address uncertainties arising from various driving conditions. Lyapunov stability, a theoretical objective in control theory, is attained by the online controller. The projected method consumes less power than both the generalised PSO and the improved PSO procedures. Researchers use simulations with the method's flexibility, practicality, and usefulness. Combining FLC with driving-cycle detection, as suggested by Wang et al. [23], may enhance fuel economy and battery life to near-optimal levels. The first step in creating a full FCV model is to design the dynamic system and the energy management system.

The goal is to minimise consumption across four typical driving cycles, and a genetic algorithm (GA) is used to optimise the centres and widths of the FLC membership functions. K-means clustering allows us to identify driving cycles, then extract and categorise defining variables. Simulation results demonstrate that the proposed method reduces equivalent hydrogen consumption by 16.55% with the GA-optimised fuzzy EMS and by 40.50% with the traditional fuzzy EMS. This means the proposed method has a good chance of enhancing the overall fuel efficiency of (PEMFCs) by calming their output. For the vehicle (FCHEV), Sun et al. [24] developed an adaptive deep reinforcement learning (DRL)- based EMS. An adaptive fuzzy filter uses a hierarchical power splitting mechanism to make the most of all available Energy. After that, researchers apply a driving behaviour recogniser and Pontryagin's minimum principle (PMP) to determine the optimal EF for each driving style. An enhanced-space DRL-based procedure is proposed that uses. When compared to the benchmark method, ECMS.

2.1. Scheme Optimisation Problem

Hybrid systems use many energy sources to meet their highest power demands. One or more renewable energy sources are integrated into this system. Power management systems (PMS) are commonly incorporated into the design of hybrid systems to determine which source to select, thereby minimising fuel consumption and maximising system dependability and performance [25]. To meet the PMS-specified power level based on the load, a hybrid system combining fuel cells, batteries, and supercapacitors uses an optimisation and control technique [26]. Hydrogen will gradually replace fossil fuels in the PEMFC's electrical Energy and the Li-ion bank's power storage system. Hydrogen consumption for a given load "C" is calculated by summing the hydrogen consumed by the fuel cell (C_FC), the battery (C_batt), and the super capacitor (C_sc). A mathematical approach for maximising efficiency in fuel use is shown in the following equation:

$$\mathbf{P_{FC} = min(C_{FC} + k_1 . C_{batt} + k_2 . C_{sc})} \tag{1}$$

Here, P_FC indicates the power generated by a fuel cell, whereas k1 and k2 reflect the penalty coefficients associated with the converter's use of hydrogen. Meanwhile, DC power is achieved by the battery converter; thus, ultracapacitor power may be disregarded during optimisation. Here, the fuel cell and the batteries share the load during each phase while the UCs are either drained or refilled with the same power from a battery bank. The resulting form of the optimisation issue is as follows:

$$\mathbf{x = [P_{FC} + k_1 . P_{batt}]} \tag{2}$$

Discovering the optimal key (x) reduces (F):

$$\mathbf{F = [P_{FC} + k_1 . P_{batt}]\Delta T} \tag{3}$$

Here, x signifies the optimal solution, k1 denotes the consequence coefficient, and DT signifies the sampling period. The coefficient is assumed to be:

$$\mathbf{k_1 = 1 - 2\mu \frac{(SoC - 0.5(SoC_{max} - SoC_{min}))}{SoC_{max} - SoC_{min}}} \tag{4}$$

The projected hydrogen practice of the cordless ($\mathbf{C_{batt}}$) can be figured by means of the influence of the cordless ($\mathbf{P_{batt}}$) and the national battery. Now, under the circumstances of equality:

$$\mathbf{P_{load} = P_{FC} + P_{batt}} \tag{5}$$

With the restraints of boundaries:

$$\mathbf{P_{fc\_min} \le P_{FC} \le P_{fc\_max}} \tag{6}$$

$$\mathbf{P_{batt\_min} \le P_{batt} \le P_{batt\_max}} \tag{7}$$

$$\mathbf{0 \le k_1 \le 100} \tag{8}$$

This multi-objective optimisation has been fully discussed in this study, and it may be the ultimate goal for any hybrid power scheme that uses hydrogen fuel and energy storage devices.

3. Modelling and Explanation of Hybrid Power Storage Scheme

Combining a PEMFC with Li-ion batteries creates a hybrid energy storage scheme (HESS). It is common practice to treat these three as a single FCHEV to ensure the load is always supplied with sufficient power. Figure 2 depicts the setup for the hybrid system study.

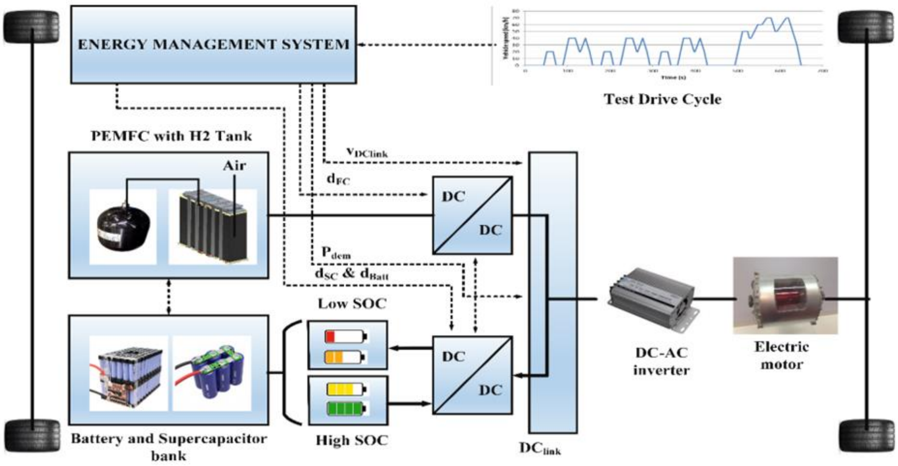

Figure 2: Hybrid electric car energy management setup

The power in this system comes from three different places: a fuel cell, a rechargeable battery, and capacitors. To raise the fuel cell's voltage to the required level and maintain it at the outputs, a DC/DC boost converter was employed. There are batteries which use a DC/DC device to change the voltage from variable to constant. To facilitate bidirectional power flow, supercapacitors, like other capacitors, are included in bidirectional converters.

3.1. Proton Exchange Membrane Fuel Cell (PEMFC)

To produce electricity from the chemical Energy contained in hydrogen fuel, a fuel cell is used; the fundamental operation of a cell is given by the chemical reaction between oxygen, as shown in Equation (9) [27]:

$$\mathbf{2H_2 + O_2 \rightarrow H_2O + electricity + heat} \quad (9)$$

Different fuel cell technologies are distinguished by the electrolytes they use. Proton exchange membrane fuel cells (PEMFCs) are another form of fuel cell. Each of the recently developed fuel cell prototypes offers distinct advantages and disadvantages. An effective model will be clear and brief [28]. In addition, a basic electrochemical notion for predicting the dynamic and static behaviour of such a fuel cell is introduced in this study [29]. This research uses a hydrogen-fuel design that accounts for the interplay between the fuel cell's voltage and the absolute amounts of hydrogen and oxygen. Table 1 presents the detailed parameters of the fuel cell stack. Oxygen and hydrogen pressures, membrane hydration temperature, and fuel cell output current all contribute to controlling the fuel cell's voltage. The formula for this model is given in Cai et al. [30]:

$$\mathbf{V_{FC} = E_{Nernst} - V_{act} - V_{ohmic} - V_{con}} \quad (10)$$

Where E_Nernst reflects the average value of the thermodynamic potential of each cell unit, as determined by Equation (11):

$$\mathbf{E_{Nernst} = 1.229 - 0.85 \times 10^{-3}(T - 298.15) + 4.308ter5 \times 10^{-5}T\left[In\left(P_{H_2}\right) + 0.5 \times In\left(P_{O_2}\right)\right]} (11)$$

Table 1: Conditions of a fuel cell

Fuel Cell Perfect Input Limits	Conditions
Voltage	52.5 V
Sum of fuel cells	65
Nominal competence stack	50%
Working fever	45 ◦C
Insignificant source pressure	1.16 fuel (bar)

Unimportant composition (%) [H2, O2, H2O (Air)]	99% H2, 95% O2, 21% H2O (air)
Response period of fuel voltage	1 s
Peak operation of O2	60%
Voltage undershoots	2 V

Here,

V_{act} = Activation drop;

$V_{ohmic} =$ Ohmic drop;

V_{con} = Concentration drop.

Hence, for N sum of cells voltage V_{stack} is labelled as:

$$V_{stack} = N.V_{FC} \tag{12}$$

The polarisation curves show how the battery voltage affects the fuel pressures. As the ideal temperature and hydrogen pressure for FCs decrease, so do the overall polarisation patterns for FCs. When oxygen and fuel are used to maintain a chemical cell, it may provide a steady stream of Energy. Due to their density, low and moderate operating temperatures, and widespread usage in automotive fuel cells [31]. Some chemical reactions that occur in FCs also limit their efficacy during peak load [32]. Consequently, these energy sources are now being incorporated into both conventional batteries and cutting-edge hybrid supercapacitor-based storage systems.

3.2. Supercapacitors

One of the main uses of supercapacitors is energy storage. A capacitance (C_{sc}) is linked to a resistance R_{sc} below this arrangement. The limits of UC are exposed in Table 2. The underneath formulation is used to control the voltage (V_{sc}) as an important part of the SC present (I_{sc}):

$$V_{sc} = V_1 - R_{sc} \times I_{sc} = \frac{Q_{sc}}{S_{sc}} - R_{sc} \times I_{sc} \tag{13}$$

where $\mathbf{Q_{sc}}$ Represents the sum of Energy stored in the cell, and Equation (14) is used to calculate the supercapacitor's output:

$$\mathbf{P_{SC}} = \frac{\mathbf{Q_{sc}}}{\mathbf{C_{sc}}} \times \mathbf{I_{SC}} - \mathbf{R_{SC}} \times \mathbf{I_{SC}^2} \tag{14}$$

Table 2: Provisions of supercapacitors

Specifications	Supercapacitor Perfect Input Limits
307 V	Flow voltage
6	Capacitors sum in series
1	Capacitor count in parallel
291.6 V	Valued voltage
0.15 ohms	DC series confrontation equivalent
15.6 F	Valued capacitance
0.4 × 10−9 m	Molecular radius
25 ◦C	Working temperature

The use of supercapacitors in such an electric vehicle's storage system requires a stack of cells, with N_S cells in series and N_p in parallel. The supercapacitor stack's capacity and resistance are calculated using Equations (15) and (16):

$$\mathbf{C_{SC}} = \mathbf{C_{elem}} . \frac{\mathbf{N_p}}{\mathbf{N_s}} \tag{15}$$

$$\mathbf{R_{SC}} = \mathbf{R_{elem}} . \frac{\mathbf{Ns}}{\mathbf{Np}} \tag{16}$$

The voltage and current of a stack are calculated using equations (17) and (18) as a reference [33]:

$$\mathbf{V_{SC}} = \mathbf{N_S}.\mathbf{V_{elem}} \tag{17}$$

$$\mathbf{I_{SC}} = \mathbf{N_P}.\mathbf{I_{elem}} \tag{18}$$

3.3. Battery

In series with such a constant resistance, the battery's design incorporates a small, regulated power source [34]. Table 3 lists key characteristics of Li-ion batteries. The voltage of a battery is given by the equation (1) $\mathbf{V_{bat}}$ (18):

$$\mathbf{V_{batt}} = \mathbf{E} - \mathbf{R_{bat}}.\mathbf{I_{bat}} \tag{19}$$

Table 3: Provisions of Li-ion battery

Provisions	Input Limits for the Battery Perfect
48 V	Negligible voltage
40 Ah	Respected capacity
40 Ah	Strongminded capacity
586.88 V	Completely charged voltage
177.4 A	Negligible discharge current
0.0172 ohms	Internal resistance
36.275 Ah	Nominal voltage capacity
527.3 Volts, 1.96 Ah	Exponential region
30 s	Response period of battery voltage

Using Equation (19), researchers can determine the regulated source voltage:

$$\mathbf{E} = \mathbf{E_0} - \mathbf{K}\frac{\mathbf{Q}}{\mathbf{Q_0} - \int \mathbf{i.dt}} + \mathbf{A.exp}(-\mathbf{B}\int \mathbf{i.dt}) \tag{20}$$

Where E is the battery's no-load voltage, E0 is some constant voltage, K is the polarisation voltage, and Q is the battery's capacity in $(\mathbf{Ah})^{-1}$.

3.4. Power Management Strategies (PMS)

A dependable PMS enables HESS to regulate its power output in response to load demand. The needs for the hybrid power management architecture developed in this work are laid forth in Table 4. The PMS heavily depends on the accumulation of fuel cell reference power.

Table 4: Power management design requirements

Supplies of Power Management Policies	
Fuel cell power $[\mathbf{P_{fcmin}} - \mathbf{P_{fcmax}}]$	1–10 KW
Battery power $[\mathbf{P_{battmin}} - \mathbf{P_{battmax}}]$	−1.2–4 KW
State of charge of battery $[\mathbf{SoC_{min}} - \mathbf{SoC_{max}}]$	60–90%
DC bus voltage $[\mathbf{V_{dcmin}} - \mathbf{V_{dcmax}}]$	250–280 V
Extreme slope of current	40 A/S

The following are among the most important guarantees that a power management system (PMS) must make:

- Lower hydrogen (H2) (gm) consumption of PEMFC
- Desired value for DC bus voltage regulation
- Monitoring battery and values
- Verifying global structure constancy
- Highly efficient system operation

- Long service life of a hybrid scheme (HESS)

Having a trustworthy PMS is the key to achieving this. The correct PMS controls the HESS's power response relative to the load. The design criteria for power management in this work are laid forth in Table 4. The PMS critically needs the fuel cell reference power to function. Different forms of premenstrual syndrome are examined in depth. The following is reported on the management of HESS power, which includes the PEMFC and SC.

3.4.1. Classical Proportional Integral (PI) Technique

The HESS provides the same amount of energy as the load. This PI method employs a PI regulator to manage the battery's SoC. The fuel cell's reference power is achieved via battery regulation utilising a controller. Since the proportional and integral rates of the input are known in advance, it is possible to predict the rated controller. When the SoC of the battery is higher, the output is reduced, and the battery is allowed to supply the entire load. When the battery's SoC falls below the target, the fuel cell kicks in to power the load. When SoC is above the mean SoC (SoC*), the PI controller ensures the battery meets its requirements and is tuned online to improve responsiveness [35]. Equation (21) Zhang et al. [35] describes the PI controller's transfer function:

$$\mathbf{P_{batt}} = \left(\mathbf{K_P} + \frac{\mathbf{K_i}}{\mathbf{S}}\right).(\mathbf{SoC}^* - \mathbf{SoC}) \qquad (21)$$

Here, the output present of the FC ($\boldsymbol{I_{FC}}$) is strong-minded in power ($\boldsymbol{P_{FC}}$), which remains from the voltage of the FC ($\boldsymbol{V_{FC}}$).

3.4.2. State Machine Control Tactic

The control method utilised by the state machine system is depicted in Figure 3. There are eight stages to executing this strategy. Using the load and (SOC) bank, the FC's power may be calculated. The SMC technique's output is the fuel cell's reference power.

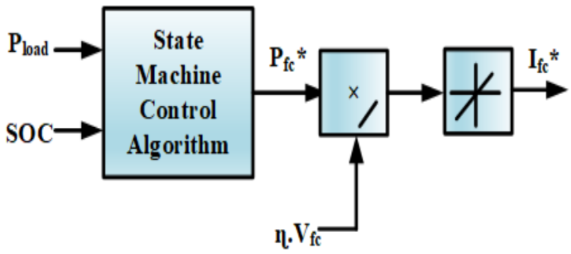

Figure 3: State machine control technique

The FC reference current is calculated by dividing the SMC output by the FC voltage and the boost converter efficiency. The SMC method requires hysteresis control during state transitions, which may alter the PMS's responsiveness to demand variations; a pattern illustrates this.

3.4.3. Frequency Decoupling Fuzzy Logic Control Structure (FDFLCS)

The fuel cell's architecture handles lower-frequency load requests, while the battery and supercapacitors provide higher-frequency requests. This scheme's main benefit is that it minimises SoC variation by bringing the Li-ion battery's mean energy closer to zero [36]. Frequency decoupling is achieved with a filter, and a fuzzy logic controller is needed to maintain the battery's charge level.

3.4.4. External Energy Expansion Approach (EEMS)

Improving HESS performance in FCHEV requires judicious use of the energy-exchange battery. This is accomplished by keeping the SC and battery within their predetermined limits, thereby reducing the hydrogen (H_2) consumption of the fuel cells. By increasing the need for batteries and SCs, this EEMS method reduces H_2 usage. Although the calculated battery energy estimate is not necessary for the EEMS method, the battery and SC cost function are. Using the DC bus voltage and battery SoC voltage as inputs, the EEMS algorithm calculates the supercapacitor and the battery reference power as outputs, as illustrated in Figure 6. Thus, the FC current (I_FC*) is used to assess the Difference between the battery power and the load power, which serves as the FC's reference power. The voltage at the SC during charging or discharging is calculated by adding the DC bus voltage (V_(dc.ref)) to the SC voltage. To solve this EEMS optimisation problem, researchers must first determine the optimal SC charge (DV) and battery power (P_batt). As shown in Equation (22), the goal function to minimise is the power delivered by sources during the interruption. Minimise:

$$\mathbf{J} = -\left(\mathbf{P_{batt}} . \Delta\mathbf{T} + \frac{1}{2}\mathbf{C_r} . \Delta\mathbf{V^2}\right) \tag{22}$$

Inequality constraints characterise key parameters and are amenable to optimisation based on power output using the EEMS:

$$\mathbf{P_{batt}} . \Delta\mathbf{T} \leq (\mathbf{SoC} - \mathbf{SoC^{min}}) . \mathbf{V_{batt}} . \mathbf{Q} \tag{23}$$

Parametric inequality restrictions are stated with respect to battery power and DC bus voltage as follows:

$$\mathbf{P_{batt}^{min}} \leq \mathbf{P_{batt}} \leq \mathbf{P_{batt}^{max}} \tag{24}$$

$$\mathbf{V_{DC}^{min}} \leq \mathbf{V_{DC}} \leq \mathbf{V_{DC}^{max}} \tag{25}$$

Here, $\mathbf{P_{batt}} . \Delta\mathbf{T}$ signifies the sampling time (DV). Cr represents the rated capacitance of SC. $\mathbf{V_{DC}^{min}}$ and $\mathbf{V_{DC}^{max}}$ Signify the bus voltage limits. $\mathbf{V_{batt}}$ indicates the battery's optimal voltage, and Q stands for the battery's rated capacity.

4. Proposed Hybrid Power Management Strategy

Adaptive-ECMS is implemented over the life of a fuel cell to reduce hydrogen consumption and extend the cell's lifespan. The core idea behind ECMS is to minimise both the equivalent and actual cells by converting electricity usage via energy storage devices into commensurate hydrogen consumption. To keep the energy sources operational, similar constraints have been imposed. The optimum function looks like this:

$$\min f_w(t) = m_{FC}(t) + m_{BA}(t) + m_{SC}(t)$$

$$\begin{cases} I_{FC}^{min} \leq I_{FC} \leq I_{FC}^{max} \\ I_{SC}^{min} \leq I_{SC} \leq I_{SC}^{max} \\ -dI_{FC} \leq \frac{I_{FC}(t) - I_{FC}(t-1)}{T} \leq dI_{FC} \end{cases} \tag{26}$$

I_{FC}^{*} Is the current standard used in fuel cells? Here, I_FC and I_SC represent the present flowing cell and the ultracapacitor, respectively; Hydrogen consumption for utilisation is denoted by f_w (t), whereas hydrogen consumption for fuel cells is denoted by m_FC (t), hydrogen consumption for batteries is denoted by m_BA (t), and hydrogen consumption for ultracapacitors is denoted by m_SC (t). Equation (10) shows how many additional penalty factors must be added to the optimisation issue of Equation (9) for the fuel cell to locate its most efficient location within the limit. To reduce energy consumption, the suggested Tugeno fuzzy controller is used to regulate the motor speed. Higher energy management and improved efficiency are achieved in the output layer of hybrid electric cars. The energy organisation system of a hybrid electric car is simulated using a Sugeno Fuzzy PI Controller. Fuzzy Logic is a form of uncertainty-providing soft computing. A Sugeno Fuzzy PI Controller provides HEV energy management. The PI control is handled by the fuzzy controller, which employs fuzzy rules. In concept, PI is not a linear regulator, but in practice, it is. The formula is:

$$\mathrm{TFPI}(t) = K_p\left(\frac{1}{I_p}\int_0^t x(t+1)dt\right) \tag{27}$$

From (27), 'TFPI(t)' indicates the result from the PI fuzzy controller. 'K_p' stands for the scalar parameters. The integrator parameter is denoted by "I_p." The input/output association of a fuzzy scheme is a linear approximation of a nonlinear procedure. Using a linearising nonlinearity, the model's operating points correspond to each fuzzy rule. Fuzzy blending is the means through which a system approach is attained. The form of the nonlinear continuous-time system is:

$$\begin{cases} x(t) = f(x(t+1), a(t), b(t)) \\ y(t) = h(x(t+1)) \end{cases} \tag{28}$$

From (28), 'f(x)' signifies the nonlinear smooth function. '$x(t+1) \in R^{n\times1}$' signifies state vector. '$B(t) \in R^{n\times1}$' labels control input. '$P(t) \in R^{n\times1}$' represents external trouble input. It is given by:

$$x(t) = \sum_{\imath=1}^{r} h_\imath(z(t))(C_\imath \dot{x}(t) + D_\imath u(t) + F_\imath v(t)) \quad (29)$$

$$y(t) = \sum_{i=1}^{r} a_i(z(t))G_i(x(t)) \quad (30)$$

From (29) and (30), 'S_i', 'D_i', 'O_i' and 'G_i' signifies continuous matrices using suitable dimensions for every fuzzy rule. '$h_i(z(t))$' designates the i^{th} normalised association function for addressing fairness. It is expressed as:

$$\sum_{i=1}^{r} a_i\left(z(t)\right) = 1 \quad (31)$$

Parameter and load disturbances are handled with fuzzy controllers. The controller's settings are adjusted so that the hybrid model continues to function as expected. The system used both an inner loop to regulate current and an external loop to regulate speed. Sugeno Fuzzy PI is used to regulate the engine's idle speed, with parameters that vary based on factors such as engine temperature and load. It is written out as:

$$Hd(t) = \sum_{j=1}^{r} In(t) + TFPI(t) * w_{h_1h_2} \quad (32)$$

From (32), the fuzzy controller output is obtained. '$w_{h_1h_2}$' weight among the hidden layer. Lastly, hidden layer 2 is the layer. The output values of the function are binary (0, 1) values. It has the following form:

$$Ou(t) = Hd(t) * w_{oh_2} \quad (33)$$

From (33), '$Ou(t)$' symbolises the output layer. 'w_{oh_2}' represents how much importance is placed on the layer. The suggested model's optimal learning rate is determined through a refined sand-cat optimisation algorithm. The following section discusses the optimised value.

4.1. Sand Cat Swarm Algorithm

Amir Seyyedabbasi and Farzad Kiani presented the intelligent optimisation algorithm, Sand Cat Swarm Optimisation (SCSO), in 2022. This system draws on wild cats' survival strategies [37]; [38]. The sand cat can hear low-frequency sounds from above or below the ground, allowing it to find prey. The ideal value in the search space is treated as prey by the algorithm, and the search agent makes incremental progress towards it by updating its location. Both a prey search and a prey assault mechanism are built into the SCSO algorithm. The technique can mimic how sand cats hunt for food using the seek-prey mechanism. The sand cat's acute hearing allows it to detect frequencies below 2 kHz during the exploratory phase. The mathematical model's sensitivity range, denoted by r_G, reduces linearly from 2 to 0 in accordance with the algorithm's underlying premise. Under the premise of 2, as described below, S_M represents the dune cat's aural characteristics as follows:

$$\overrightarrow{r_G} = s_M - \left(\frac{S_M \times iter_c}{iter_{max}}\right) \quad (34)$$

R, outlined below, is the primary metric for gauging the readiness of a project to go from exploration to development:

$$\vec{R} = 2 \times \overrightarrow{r_G} \times rand(0,1) - \overrightarrow{r_G} \quad (35)$$

The search space is seeded at random inside the parameters you provide. Each active search agent's position is updated during the search phase from a completely random starting position. This allows the search agent to expand its horizons and investigate uncharted regions of the search space. Each cat has a variety, which is defined such that they do not all converge to a single optimal solution:

$$\vec{r} = \overrightarrow{r_G} \times rand(0,1) \ (\quad (36)$$

With the SCSO procedure, the sand cat searches for alternative best prey positions, finds a new local optimum in a new-fangled search area, and obtains a position and the prey site, all while maintaining complexity. The following is a mathematical representation of the searching procedure:

$$\vec{P}os(t+1) = \vec{r}.\left(\vec{P}os_b(t) - rand(0,1)\right).\vec{P}os_c(t) \quad (37)$$

Where: $\vec{P}os_b$ is the optimal solution, $\vec{P}os_c$ is one's current sensitivity range. The sand cat population's prey attack process is defined as follows, and the SCSO algorithm launches its assaults on prey at the conclusion of the prey search:

$$\vec{P}os_{md} = \left|rand(0,1).\vec{P}os_b(t) - \vec{P}os_c(t)\right| \quad (38)$$

$$\vec{P}os(t+1) = \vec{P}os_b(t) - \vec{r}.\vec{P}os_{md}.\cos(\theta) \quad (39)$$

Where: Pos_b is the best site, Pos_c is the current site, and Pos_{md} Is the random site:

$$\vec{P}os(t+1) = \begin{cases} \vec{P}os_b(t) - \vec{P}os_{rnd}.\cos(\theta).\vec{r} & |R| \leq 1 \\ \vec{r}.\left(\vec{P}os_b(t) - rnd(0,1).\vec{P}os_c(t)\right) & |R| > 1 \end{cases} \quad (40)$$

During the prospecting and mining stages, the site of each sand cat is updated according to Equation (40). When $R \leqslant 1$, the sand cats are entrusted with discovering new global solutions when not directed to attack their prey.

4.2. Enhanced Sand Cat Swarm Optimization

4.2.1. Logistic Chaos Mapping

The optimisation impact of the population intelligence algorithm depends heavily on the initial locations of the entities in the population [39]. Logistic tent mapping, Hanon mapping, and Chebyshev chaos mapping are all examples of popular chaotic mapping techniques. In this study, researchers select the logistic mapping because it outperforms alternative chaotic mappings in terms of ergodicity, autocorrelation, and mutual correlation. To improve algorithmic performance and optimisation precision, a logistic chaos map is used to initialise the population, creating a more uniform distribution of individuals [40]. Here is the equation:

$$x_{k+1} = \mu x_k(1 - x_k) \quad (41)$$

Where $\mu \in (0,4)$, kis the sum of repetitions, and $x \in (0, 1)$. With the early value of x_0The evidence of the chaotic nature is that μ takes $[3.569699, 4.0]$ and the order of chaotic conditions is convergent.

4.2.2. Water Wave Dynamic Issue

The SCSO approach is inaccurate and struggles to adapt to multi-peaked multivariate functions. In this algorithm, rG drops linearly from 2 to 0 during the iterative phase. The algorithm's adaptability to newly acquired complexity is enhanced, and the likelihood of finding a satisfactory solution is increased by introducing a water-wave dynamic evolution component that leverages the inherent uncertainty in water-wave dynamics. Using water wave dynamics introduces an element of uncertainty that allows the population to search over a larger region, which in turn reduces the blindness of other personalities following, improves information conversation and learning among populations, keeps populations diverse, and helps the algorithm avoid convergence. Simultaneously, the magnitude reduction of rG is modulated by a control factor k, as stated in Equation (42), in the mathematical model (Figure 4).

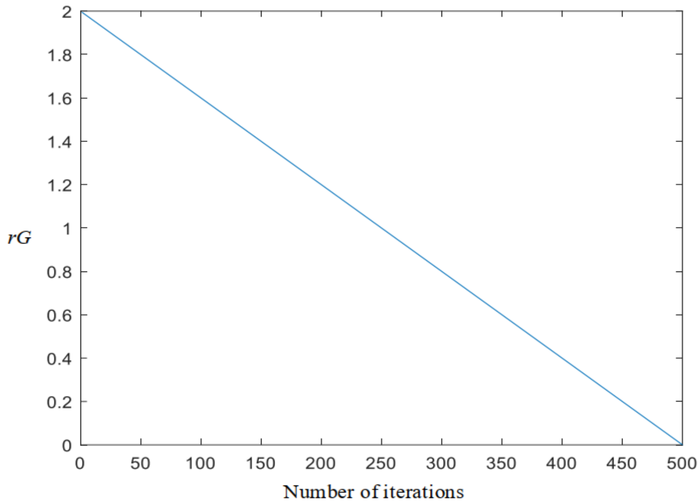

Figure 4: The unique rG repetition curve

$$rG = 2.s.\exp\left(\frac{-t}{T}\right)^{k}.r \tag{42}$$

Where: s is an accidental figure and $s \in [-1, 1]$; r is a purpose. The larger k is, the more rG increases, and vice versa for big k. Figures 3 and 4 illustrate an assessment between the initial rG and the water wave factor as a function of the number of repeats.

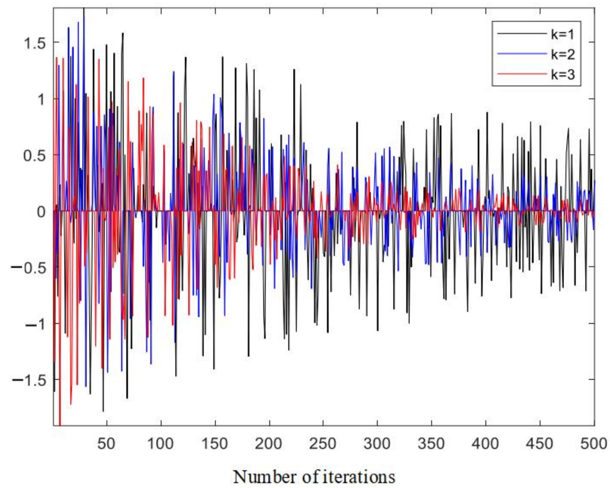

Figure 5: Water wave dynamic influences for diverse values of k

4.2.3. Adaptive Weights

Appropriate inertia weights can efficiently coordinate the algorithm's shift from global search to local exploitation, thereby accelerating and fine-tuning the search for the objective optimisation function and enhancing convergence speed and accuracy. When doing a local search for the optimal, the sand cat used Equation (37). If the sand cat is constrained to search for an optimum within the area of Equation (37), it will only be able to seek a solution that is very close to the optimal one. This study introduces a novel weighted adaptive method that improves local optimisation of the sand cat by reweighting the current sand cat location using a minimal adaptive weighting as it approaches the goal. Equation (43) displays the adaptive weighting formula, while Equation (44) displays the refined version of Equation (37):

$$w = \sin\left(\frac{\pi.t}{2.\mathrm{iter}_{max}} + \pi\right) + 1 \tag{43}$$

$$\vec{P}os(t+1) = w.\vec{r}.\left(\vec{P}os_{bc}(t) - \mathrm{rand}(0,1)\right).Pos_{c}(t) \tag{44}$$

4.2.4. Golden Sine

In Wang et al. [41], a novel intelligent algorithm, the golden sine algorithm (goldenSA), is developed based on a concept related to the sine function. It benefits from fast search speed, easy parameter tuning, and high resilience. When paired with the golden partition coefficient, the unique connection circle enables the golden-SA method to perform iterative search; the unit circle simulation algorithm, meanwhile, scans the sine function to investigate the search space. In the fourth century B.C., the ancient Greek mathematician Eudoxus created the notion of the golden mean. Since the golden mean's contraction step is predetermined, it does not require gradient information and can be computed in a single iteration. Therefore, the extreme or lowest value of the function may be found more rapidly by combining the sine function with the golden mean. The method is protected against a trap known as a local optimum by the repeated nature of the sine search approach. Golden-SA may be mathematically modelled as shown in Equation (45):

$$X_i^{t+1} = X_i^t.|\sin(R_1)| + R_2.\sin(R_1).|x_1.P_i^t - x_2.x_i^t| \tag{45}$$

Where t is the number of iterations, R_1 is a random sum in the range [0,2], and R_2 is a random number in the range [0,] that represents the distance section coefficients that are used to constrain the search space and guide individuals to converge to P_it is individual. Search intervals a and b are used to calculate the golden-section coefficients x1 = a (1-)+b and x2 = a+b (1-). The golden section ratio is about 0.618033.

4.2.5. ISCSO Implementation Stages

In this article, researchers detail the precise procedures to be followed to achieve the enhancements mentioned above to ISCSO:

- **Step 1:** Set population size N, spatial boundaries ub and lb, and the extreme sum of iterations Tm to their initial values before running the sand cat swarm algorithm.
- **Step 2:** Apply the logistical equation (41) as a starting point for the population.
- **Step 3:** Determine how much each person is worth in terms of fitness.
- **Step 4:** In lieu of Eqs. (34) and (37), write Eqs. (42) and (44).
- **Step 5:** Adjust the coordinates using Equations (39).
- **Step 6:** Adjust the coordinates in light of Equation (45).
- **Step 7:** Check whether you've exhausted all possible iterations. So, the results are the best possible place for one person in the world; if not, go to Step 3.

This allows hybrid electric vehicles to have effective energy management systems with low electrical consumption.

5. Results and Discussion

Minimising fuel usage in a hybrid electric vehicle (i.e., an electric automobile) is the goal of the experimental assessment of a model built in MATLAB Simulink on a 3.4 GHz Intel Core i3 CPU, 4GB RAM, and Windows 7. Hybrid electric cars have an energy management system that operates most efficiently when the vehicle is moving at its maximum speed. The energy management is put through its paces on both short and extended trips. The hybrid electric cars' improved fuel economy was the result of an energy management scheme. It is crucial in distributing electricity from the engine to the battery. The power split enhanced efficiency and power regulation. Parameter selection for the proposed perfect is outlined in Table 5.

Table 5: Selection of parameters using ISCSO for the controller

Parameters	Parametric Values
Particle Population	100
Convergence Acceptance	104
Particle Population	100
Leaming rate	0.3
Sum of input neurons	5
Sum of the early hidden neurons	5
Extreme Iteration	100
FIS	Sugeno
Sum of trial runs	30

Parameter values for a high-performing energy management system using a Sugeno Fuzzy PI controller are shown in Figure 5.

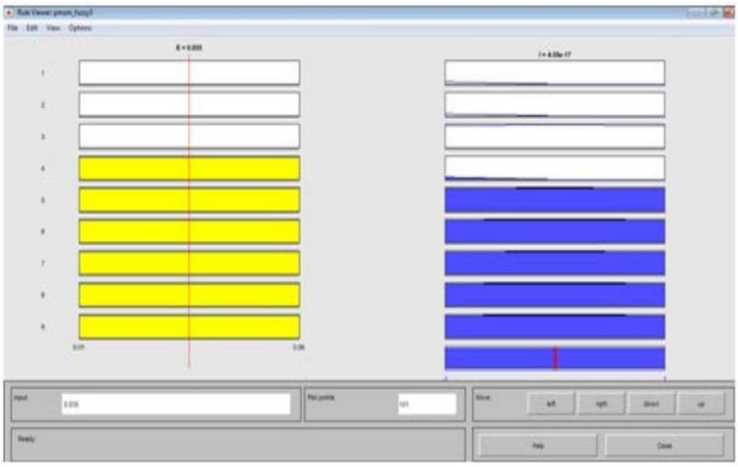

Figure 6: Fuzzy Sugeno PI controller

Figure 5 shows the consequences of the Sugeno Fuzzy PI Controller. The figure shows e=0.035 and 4.55*10-16 error integral. Figure 6 and Table 6 show hydrogen consumption (Ipm and grammes).

Table 6: Hydrogen consumption of each scheme

	SMC	FDFLC	ECMS	PI	EEMS	Proposed
System Efficiency	78.52	74.77	72.51	73.77	74.15	84.47
Hydrogen consumption	32.063	32.1897	35.9708	31.6335	30.1774	20.93

In the above table, 6 represents the Hydrogen consumption of different schemes. In the following, the Hydrogen consumption of the PI model reached 31.6335, the SMC model reached 32.063, the FDFLC scheme reached 32.1897, the ECMS reached 35.9708, the EEMS reached 30.1774, and finally the proposed model reached 20.93y. And the System Efficiency of the PI model reached 73.77, the SMC model reached 78.52, the FDFLC scheme reached 74.77, the ECMS reached 72.51, the EEMS reached 74.15, and the proposed model reached 84.47, respectively (Figure 7).

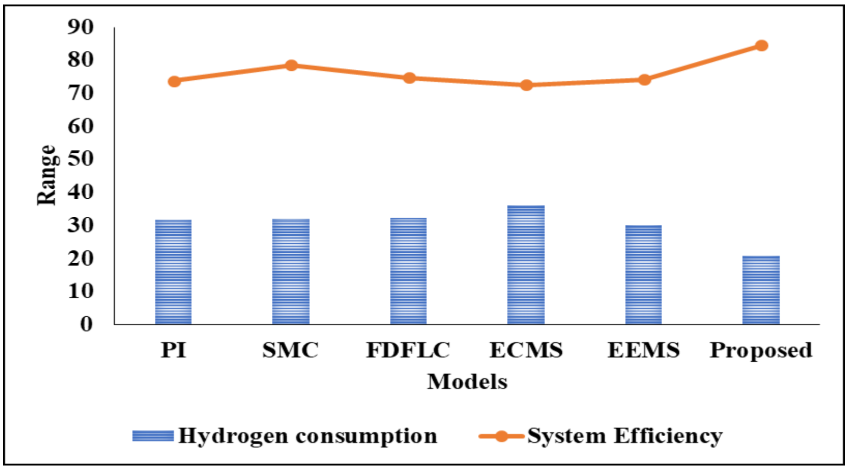

Figure 7: Arrangement efficiency and hydrogen ingestion for each arrangement

Table 7 below shows hydrogen consumption in grams. At 0 grams, the PI model reached 0, and the other compared models also reached 0. The other compared models are elaborated below. In the 50 case, the PI model reached 7, the SMC model reached 6, the FDFLC model reached 5, the ECMS range reached 5, the EEMS model reached 4, and the proposed model reached 3 (Figure 8).

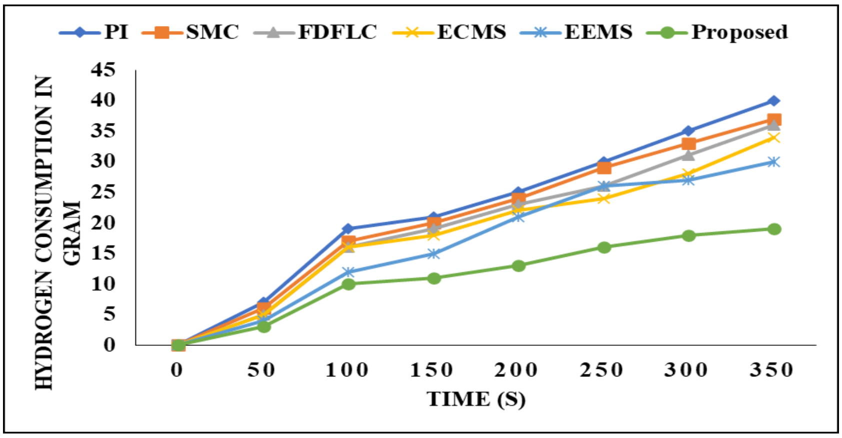

Figure 8: Hydrogen ingesting in grams for various tactics

In the 100-gram case, the PI model reached 19, the SMC model reached 17, the FDFLC model reached 16, the ECMS model reached 16, the EEMS model reached 12, and the proposed model reached 10. In the 150-gram case, the PI model reached 21, the SMC model reached 20, the FDFLC model reached 19, the ECMS model reached 18, the EEMS model reached 15, and the proposed model reached 11.

Table 7: Hydrogen consumption in terms of grams

Grams	PI	SMC	FDFLC	ECMS	EEMS	Proposed
0	0	0	0	0	0	0
50	7	6	5	5	4	3
100	19	17	16	16	12	10
150	21	20	19	18	15	11
200	25	24	23	22	21	13
250	30	29	26	24	26	16
300	35	33	31	28	27	18
350	40	37	36	34	30	19

In the 200-gram case, the PI model reached 25, the SMC model reached 24, the FDFLC model reached 23, the ECMS model reached 22, the EEMS model reached 21, and the proposed model reached 13. In the 250-gram case, the PI model reached 30, the SMC model reached 29, the FDFLC model reached 26, the ECMS model reached 24, the EEMS model reached 26, and finally, the proposed model reached 16. In the 300-gram case, the PI model reached 35, the SMC model reached 33, the FDFLC model reached 31, the ECMS model reached 28, the EEMS model reached 27, and the proposed model reached 18y. In the 350-gram range, the PI model reached 40, another SMC model reached 37, the FDFLC model reached 36, the ECMS range reached 34, the EEMS model reached 30, and finally, the proposed model reached 19.

Table 8: Hydrogen consumption in IPM for deliberate approaches

Ipm	PI	SMC	FDFLC	ECMS	EEMS	Proposed
0	0	0	0	0	0	0
50	19	8	10	12	9	5
100	98	90	88	96	80	78
150	98	90	88	96	80	78
200	70	8	10	12	9	5
250	98	90	87	96	80	78
300	98	90	86	96	80	78
350	65	62	63	70	64	5

In the above Table 8 represents the Hydrogen consumption in IPM for the studied approaches. In the 0-gram values, all the model results are 0. And for the 50 Ipm, the PI model reached 19, the SMC model reached 8, the FDFLC model reached 10, the ECMS model reached 12, the EEMS model reached 9, and the proposed model reached 5. And another 100 Ipm, the PI model reached 98, the SMC model reached 90, the FDFLC model reached 88, the ECMS model reached 96, the FDFLC model reached 80, and lastly, the proposed model reached 78, respectively (Figure 9).

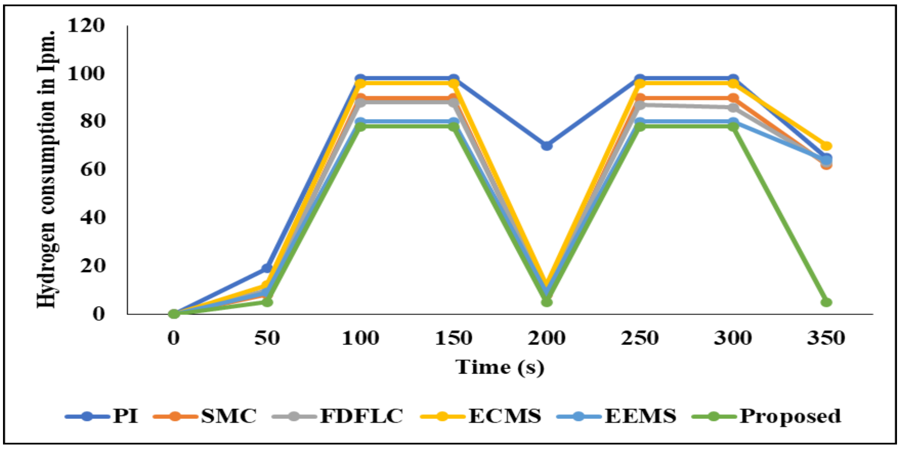

Figure 9: Consumption of hydrogen in terms of IPM

And another 150 Ipm, the PI model reached 98, the SMC model reached 90, the FDFLC model reached 88, the ECMS model reached 96, the EEMS model reached 80, and the proposed model reached 78, respectively. And another 200 Ipm, the PI model reached 70, the SMC model reached 8, the FDFLC model reached 10, the ECMS model reached 12, the EEMS model reached 9, and the proposed model reached 5. And another 250 Ipm, the PI model reached 98, the SMC model reached 90, the FDFLC model reached 87, the ECMS model reached 96, the EEMS model reached 80, and the proposed model reached 78, respectively. And another 300 Ipm, the PI model reached 98, the SMC model reached 90, the FDFLC model reached 86, the ECMS model reached 96, the EEMS model reached 80, and the proposed model reached 78, respectively. And another 350 Ipm, the PI model reached 65, the SMC model reached 62, the FDFLC model reached 63, the ECMS model reached 70, the EEMS model reached 64, and the proposed model reached 5. In the table below, Table 9 represents the Dissimilarity in fuel cell voltage. In this analysis, at time 0, the proposed model reached 56, respectively. At the age of 50, the proposed model reached 46, respectively.

Table 9: Variation in fuel cell input voltage

Time (s)	Proposed
0	56
50	46
100	42
150	42
200	46
250	42
300	48
350	49

In 100 years, the proposed model reached 42, respectively. In 150, the proposed model reached 42, respectively. In 200, the proposed model reached 46, respectively. In 250, the proposed model reached 42, respectively. In the year 300, the proposed model reached 48, respectively. In the year 350, the proposed model reached 49, respectively (Figure 10).

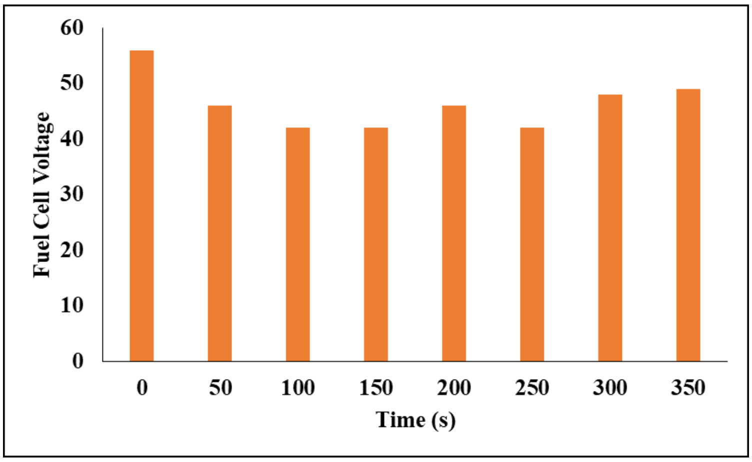

Figure 10: Fuel cell voltage

In the table below, Table 10 represents the Difference in fuel cell current. At time 0, the proposed cell input current reached 20. In the 50-time range, the proposed cell input current reached 25. In the 100-time range, the proposed cell input current reached 220. In the 150-time range, the proposed cell input current reached 220.

Table 10: Variation in fuel cell input current

Time (s)	Proposed
0	20
50	25
100	220
150	220
200	150
250	220
300	80
350	25

In the 200-time range, the proposed cell input current reached 150. In the 250-time range, the proposed cell input current reached 220. In the 300-time range, the proposed cell input current reached 80. In the 350-time range, the proposed cell input current reached 25 (Figure 11).

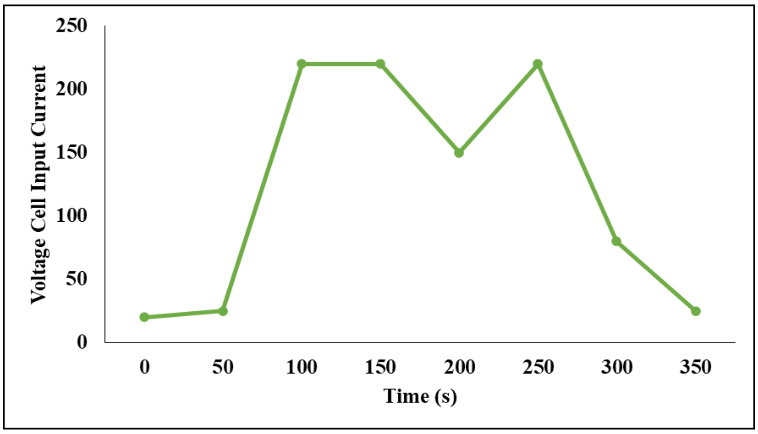

Figure 11: Graphical representation of input current

Table 11 below represents the Calculation analysis on various drive cycles. In the Criteria for PMS in State of charge battery (%) in duty cycle of HWFET (Economy Test Cycle) as PI reached the 70.51 and the SMC reached 70-54 and the FDFC reached the 70.54 and also the ECMS model reached the 70–54 and another EEMS model reached 70–59 and finally the Proposed model reached 70–58 respectively. And another Consumption of H2 (g), the PI reached the 31.63, and the SMC reached 70-54, and the FDFC reached the 35.97, and also the ECMS model reached the 70–54, and another EEMS model reached 70–59 and finally the Proposed model reached 22-93, respectively.

Table 11: Calculation analysis on various drive cycles

Drive Cycle	Standards for PMS	SMC	ECMS	EEMS	PI	FDFC	Projected
HWFET (Highway Fuel Economy Test Cycle)	State of battery charge (%)	70–54	70–54	70–59	70–51	70.54	70–58
	Consumption of H2 (g)	32.06	35.97	30.17	31.63	32.97	22.93
	Overall efficiency (%)	78.52	72.51	74.15	73.77	74.77	80.47
	Stress on battery (s)	21.91	24.6	22.4	22	24.6	23.7
	Stress on fuel cell (s)	22.59	23.42	18.6	20.42	22.04	15.8
	Stress on ultracapacitor (s)	34.7	37.84	35.9	35.92	37.84	36.76

And another Overall efficiency (%), the PI reached 73.77, and the SMC reached 70-54, and the FDFC reached 70.54 and also the ECMS model reached 71.51, and another EEMS model reached 70–59, and finally the Proposed model reached 70–58, respectively. And another Stress on battery(s): the PI reached 22, the SMC reached 21.91, the FDFC reached 24.6, the ECMS model reached 22.4, another EEMS model reached 70–59, and finally the Proposed model reached 23.7, respectively. And another Stress on fuel cell(s): the PI reached 20.42, the SMC reached 22.59, and the FDFC reached 22.04; the ECMS model reached 23.42, and another EEMS model reached 18.6; and finally, the Proposed model reached 15.8, respectively. And another Stress on ultracapacitor (s), the PI reached 35.92, the SMC reached 34.7, and the FDFC reached 37.84 and also the ECMS model reached 37.84, and another EEMS model reached 35.9, and finally the Proposed model reached 36.76, respectively.

Table 12: Analysis of the proposed model on WLTC

Drive Cycle	Standards for PMS	SMC	FDFC	EEMS	PI	ECMS	Projected
WLTC (Worldwide Harmonized Light Vehicle Test Cycles) battery (%)	State of charge battery (%)	70–54	70.53	70–59	70–52	70–53	70–59
	Feasting of H2 (g)	30.83	33.29	33.19	31.5	38.13	22.74
	Overall efficiency (%)	77.28	71.83	78.19	76.16	72.11	81.29
	Stress on battery (s)	24.81	27.9	24.46	28	29.4	24.38
	Stress on fuel cell (s)	23.19	21.84	19.23	24.23	27.17	19.82
	Stress on ultracapacitor (s)	32.45	31.93	37.1	36.12	34.92	31.15

In the above Table 12 represents the analysis of the proposed model on WLTC. In the analysis, the WLTC (Worldwide Harmonised Light Vehicle Test Cycles) drive cycle is determined. In the analysis of public battery charge (%), the PI reached 70.52, and the SMC reached 70-54, and the FDFC reached 70-53, and also the ECMS model reached 70–59, and another EEMS model reached 70–59, and finally the Proposed model reached 70–59 respectively. And another piece of Consumption of H2 (g): the PI reached 31.5, the SMC reached 30.83, the FDFC reached 33.29, the ECMS model reached 38.13, another EEMS model reached 33.19, and the Proposed model reached 22.74, respectively. After that, the Overall efficiency (%) the PI reached 76.16, the SMC reached 77.28, the FDFC reached 71.83, the ECMS model reached 72.11, another EEMS model reached 70–59, and finally, the Proposed model reached 81.29, respectively. On the other hand, for Stress on battery(s), the PI reached 28, the SMC reached 24.81, the FDFC reached 27.9, the ECMS model reached 29.4, another EEMS model reached 24.46, and finally the Proposed model reached 24.38, respectively. Also, the Stress on fuel cell(s) was 24.23, the SMC was 23.19, the FDFC was 21.84, the ECMS model was 27.17, another EEMS model was 19.23, and the Proposed model was 19.82, respectively. And finally, the Stress on ultracapacitor(s) reached 36.12, the SMC reached 32.45, the FDFC reached 31.93, the ECMS model reached 34.92, another EEMS model reached 37.1, and the Proposed model reached 31.15, respectively.

6. Conclusion

With the primary power source being a PEMFC-based UC, this research proposes a Sugeno Fuzzy Controller-based ECMS-integrated control policy for cars to preserve maximum fuel. The battery power penalty coefficients govern SoC in the ECMS, which uses a cost-function-based optimisation method. This method of optimisation undervalues UC's potential. To recharge the UCs with the same amount of energy from the battery bank after they have been depleted, the battery bank's converters control the DC bus voltage profile. A battery and FC are used to maintain load balance across a load cycle. Compared to traditional control systems, the high tracking speed and low error signal of the controller based on the Sugeno Fuzzy Controller make it ideal for keeping up with the ever-changing energy demand. Since battery life can be extended through constant monitoring, HEVs will operate better and more reliably. By reducing the battery's load, the suggested HESS active power system provides better control throughout an EV's driving cycle. As a result, the system is easier to regulate. The active power splitting among the battery and ultracapacitor hybrid source is demonstrated by the simulation results in several different modes depending on the (SOC) of the device, the peak load needed, the instantaneous variations in an EV load, and the load voltage restrictions. Extending the range of EVs is a potential goal of future research that might benefit from studying the regeneration duration of ultracapacitors using an EV load outline during the retro.

Acknowledgement: The authors gratefully acknowledge the support of New Horizon College of Engineering, Nitte Meenakshi Institute of Technology (NMIT), Saranathan College of Engineering, Karunya Institute of Technology and Science, and Amity University Dubai. Their collective guidance and resources enabled the successful completion of this research.

Data Availability Statement: The study utilises a dataset related to the Hybrid Power Management Strategy using SFO-based Improved Sand Cat Swarm Optimisation to enhance fuel economy in Hybrid Electric Vehicle (HEV) applications. The data supporting the findings of this study are available from the corresponding author upon reasonable request.

Funding Statement: The authors affirm that this research and the preparation of the manuscript were carried out without any external funding or financial assistance.

Conflicts of Interest Statement: All authors declare that they have no competing interests that could influence the outcomes, interpretations, or presentation of this study.

Ethics and Consent Statement: This study was conducted in accordance with ethical guidelines, and all necessary approvals were obtained. Informed consent was collected from all participating individuals and collaborating organisations before data acquisition.

References

1. F. Zhang, L. Wang, S. Coskun, H. Pang, Y. Cui, and J. Xi, "Energy management strategies for hybrid electric vehicles: Review, classification, comparison, and outlook," *Energies*, vol. 13, no. 13, p. 3352, 2020.
2. T. Liu, W. Tan, X. Tang, J. Zhang, Y. Xing, and D. Cao, "Driving conditions-driven energy management strategies for hybrid electric vehicles: A review," *Renewable and Sustainable Energy Reviews*, vol. 151, no. 11, p. 111521, 2021.
3. C. Yang, M. Zha, W. Wang, K. Liu, and C. Xiang, "Efficient energy management strategy for hybrid electric vehicles/plug-in hybrid electric vehicles: Review and recent advances under intelligent transportation system," *IET Intelligent Transport Systems*, vol. 14, no. 7, pp. 702–711, 2020.

4. J. Zhou, S. Xue, Y. Xue, Y. Liao, J. Liu, and W. Zhao, "A novel energy management strategy of hybrid electric vehicle via an improved TD3 deep reinforcement learning," *Energy*, vol. 224, no. 6, p. 120118, 2021.
5. H. He, Y. Wang, J. Li, J. Dou, R. Lian, and Y. Li, "An improved energy management strategy for hybrid electric vehicles integrating multistates of vehicle-traffic information," *IEEE Transactions on Transportation Electrification*, vol. 7, no. 3, pp. 1161–1172, 2021.
6. Q. Zhou and C. Du, "A quantitative analysis of model predictive control as energy management strategy for hybrid electric vehicles: A review," *Energy Reports*, vol. 7, no. 11, pp. 6733–6755, 2021.
7. G. Du, Y. Zou, X. Zhang, L. Guo, and N. Guo, "Heuristic energy management strategy of hybrid electric vehicle based on deep reinforcement learning with accelerated gradient optimization," *IEEE Transactions on Transportation Electrification*, vol. 7, no. 4, pp. 2194–2208, 2021.
8. J. Hu, D. Liu, C. Du, F. Yan, and C. Lv, "Intelligent energy management strategy of hybrid energy storage system for electric vehicle based on driving pattern recognition," *Energy*, vol. 198, no. 5, p. 117298, 2020.
9. W. Lee, H. Jeoung, D. Park, T. Kim, H. Lee, and N. Kim, "A real-time intelligent energy management strategy for hybrid electric vehicles using reinforcement learning," *IEEE Access*, vol. 9, no. 5, pp. 72759–72768, 2021.
10. Q. Zhou and C. Du, "A two-term energy management strategy of hybrid electric vehicles for power distribution and gear selection with intelligent state-of-charge reference," *Journal of Energy Storage*, vol. 42, no. 10, p. 103054, 2021.
11. S. Hou, H. Yin, Y. Ma, and J. Gao, "Energy management strategy of hybrid electric vehicle based on ECMS in intelligent transportation environment," *IFAC-PapersOnLine*, vol. 54, no. 10, pp. 157–162, 2021.
12. Q. Zhang and X. Fu, "A neural network fuzzy energy management strategy for hybrid electric vehicles based on driving cycle recognition," *Applied Sciences*, vol. 10, no. 2, p. 696, 2020.
13. J. Li, X. Wu, S. Hu, and J. Fan, "A deep reinforcement learning based energy management strategy for hybrid electric vehicles in connected traffic environment," *IFAC-PapersOnLine*, vol. 54, no. 10, pp. 150–156, 2021.
14. P. S. P. Krishna, N. S. Jayalakshmi, and A. Kedlaya, "Energy management strategies for hybrid energy storage system in electric vehicles: A review," *in Proc. 2020 IEEE International Conference on Electronics, Computing and Communication Technologies (CONECCT)*, Bangalore, India, 2020.
15. H. He, Y. Wang, R. Han, M. Han, Y. Bai, and Q. Liu, "An improved MPC-based energy management strategy for hybrid vehicles using V2V and V2I communications," *Energy*, vol. 225, no. 6, p. 120273, 2021.
16. P. M. Estrada, D. de Lima, P. H. Bauer, M. Mammetti, and J. C. Bruno, "Deep learning in the development of energy management strategies of hybrid electric vehicles: A hybrid modeling approach," *Applied Energy*, vol. 329, no. 1, p. 120231, 2023.
17. A. Alsharif, C. W. Tan, R. Ayop, A. Al Smin, A. A. Ahmed, F. H. Kuwil, and M. M. Khaleel, "Impact of electric vehicle on residential power distribution considering energy management strategy and stochastic Monte Carlo algorithm," *Energies*, vol. 16, no. 3, p. 1358, 2023.
18. H. Zhang, J. Peng, H. Dong, H. Tan, and F. Ding, "Hierarchical reinforcement learning based energy management strategy of plug-in hybrid electric vehicle for ecological car-following process," *Applied Energy*, vol. 333, no. 3, p. 120599, 2023.
19. Y. Huang, H. Hu, J. Tan, C. Lu, and D. Xuan, "Deep reinforcement learning based energy management strategy for range-extended fuel cell hybrid electric vehicle," *Energy Conversion and Management*, vol. 277, no. 2, p. 116678, 2023.
20. Y. Liu, Y. Wu, X. Wang, L. Li, Y. Zhang, and Z. Chen, "Energy management for hybrid electric vehicles based on imitation reinforcement learning," *Energy*, vol. 263, no. 1, p. 125890, 2023.
21. X. Sun, J. Fu, H. Yang, M. Xie, and J. Liu, "An energy management strategy for plug-in hybrid electric vehicles based on deep learning and improved model predictive control," *Energy*, vol. 269, no. 4, p. 126772, 2023.
22. S. Abd-Elhaleem, W. Shoeib, and A. A. Sobaih, "A new power management strategy for plug-in hybrid electric vehicles based on an intelligent controller integrated with CIGPSO algorithm," *Energy*, vol. 265, no. 2, p. 126153, 2023.
23. Y. Wang, Y. Zhang, C. Zhang, J. Zhou, D. Hu, F. Yi, Z. Fan, and T. Zeng, "Genetic algorithm-based fuzzy optimization of energy management strategy for fuel cell vehicles considering driving cycles recognition," *Energy*, vol. 263, no. 1, p. 126112, 2023.
24. H. Sun, F. Tao, Z. Fu, A. Gao, and L. Jiao, "Driving-behavior-aware optimal energy management strategy for multi-source fuel cell hybrid electric vehicles based on adaptive soft deep-reinforcement learning," *IEEE Transactions on Intelligent Transportation Systems*, vol. 24, no. 4, pp. 4127–4146, 2023.
25. S. Mirjalili, S. M. Mirjalili, and A. Lewis, "Grey wolf optimizer," *Advances in Engineering Software*, vol. 69, no. 3, pp. 46–61, 2014.
26. H. Rezk, M. Al-Oran, M. R. Gomaa, M. A. Tolba, A. Fathy, M. A. Abdelkareem, A. G. Olabi, and A. H. M. El-Sayed, "A novel statistical performance evaluation of most modern optimization-based global MPPT techniques for a partially shaded PV system," *Renewable and Sustainable Energy Reviews*, vol. 115, no. 11, p. 109372, 2019.
27. N. Ding, K. Prasad, and T. T. Lie, "Design of a hybrid energy management system using designed rule-based control strategy and genetic algorithm for the series-parallel plug-in hybrid electric vehicle," *International Journal of Energy Research*, vol. 45, no. 2, pp. 1627–1644, 2021.

28. M. R. Nalim, R. Vasudevan, and S. Rahatekar, “Advances in Automotive Technologies: Select Proceedings of ICPAT 2019,” *Springer*, Singapore, 2020.
29. X. Zhang, L. Guo, N. Guo, Y. Zou, and G. Du, “Bi-level energy management of plug-in hybrid electric vehicles for fuel economy and battery lifetime with intelligent state-of-charge reference,” *Journal of Power Sources*, vol. 481, no. 1, p. 228798, 2021.
30. C. H. Cai, D. Du, and Z. Y. Liu, “Battery state-of-charge (SOC) estimation using adaptive neuro-fuzzy inference system (ANFIS),” *in Proc. 12th IEEE International Conference on Fuzzy Systems, 2003. FUZZ '03*, St. Louis, Missouri, United States of America, 2003.
31. R. B. Shaik and E. V. Kannappan, “Application of adaptive neuro-fuzzy inference rule-based controller in hybrid electric vehicles,” *Journal of Electrical Engineering and Technology*, vol. 15, no. 6, pp. 1937–1945, 2020.
32. P. Li, X. Jiao, and Y. Li, “Adaptive real-time energy management control strategy based on fuzzy inference system for plug-in hybrid electric vehicles,” *Control Engineering Practice*, vol. 107, no. 2, p. 104703, 2021.
33. D. Karaboga and E. Kaya, “Adaptive network-based fuzzy inference system (ANFIS) training approaches: A comprehensive survey,” *Artificial Intelligence Review*, vol. 52, no. 1, pp. 2263–2293, 2019.
34. F. Zhang, X. Hu, R. Langari, L. Wang, Y. Cui, and H. Pang, “Adaptive energy management in automated hybrid electric vehicles with flexible torque request,” *Energy*, vol. 214, no. 1, p. 118873, 2021.
35. L. Zhang, X. Ye, X. Xia, and F. Barzegar, “A real-time energy management and speed controller for an electric vehicle powered by a hybrid energy storage system,” *IEEE Transactions on Industrial Informatics*, vol. 16, no. 10, pp. 6272–6280, 2020.
36. Q. Zhang and X. Fu, “A Neural Network Fuzzy Energy Management Strategy for Hybrid Electric Vehicles Based on Driving Cycle Recognition,” *Applied Sciences*, vol. 10, no. 2, p. 696, 2020.
37. A. Seyyedabbasi and F. Kiani, “Sand Cat swarm optimization: A nature-inspired algorithm to solve global optimization problems,” *Engineering Computations*, vol. 39, no. 4, pp. 2627–2651, 2022.
38. D. Wu, H. Rao, C. Wen, H. Jia, Q. Liu, and L. Abualigah, “Modified Sand Cat Swarm Optimization Algorithm for solving constrained engineering optimization problems,” *Mathematics*, vol. 10, no. 22, p. 4350, 2022.
39. T. Dokeroglu, E. Sevinc, T. Kucukyilmaz, and A. Cosar, “A survey on new generation metaheuristic algorithms,” *Computers and Industrial Engineering*, vol. 137, no. 11, p. 106040, 2019.
40. C. Zhang and S. Ding, “A stochastic configuration network based on chaotic sparrow search algorithm,” *Knowledge-Based Systems*, vol. 220, no. 5, p. 106924, 2021.
41. J. Wang, Y. Li, G. Hu, and M. Yang, “An enhanced artificial hummingbird algorithm and its application in truss topology engineering optimization,” *Advanced Engineering Informatics*, vol. 54, no. 10, p. 101761, 2022.